Tribology Letters (2024) 72:11
https://doi.org/10.1007/s11249-023-01815-3

ORIGINAL PAPER

Bio-bearings: Numerical Model of the Solid Lubricant in the Leg Joints of Insects

Alexander E. Filippov[1] · Konstantin Nadein[1] · Stanislav N. Gorb[1] · Alexander Kovalev[1]

Received: 8 September 2023 / Accepted: 22 November 2023 / Published online: 12 December 2023

Abstract
The proposed model describes the behavior of the lubricant particles at the interface between two surfaces for a group of cylindrical semi-solid lubricant fragments observed in a real beetle leg joint. It is shown that the lubricant particles may maintain a gap between joint surfaces at load. At the regular shear motion, such randomly oriented particles are reorienting perpendicular to the shear and function as a rolling bearing: the system demonstrates the lowest energy loss and lowest friction. At an increased load, the friction non-linearly increases, because of an increase of the particles' eccentricity. Finally, at some load, the particle rotation stops, friction switches from the rolling to the sliding regime and increases significantly.

Keywords Tribology · Rolling friction · Interface · Load

1 Introduction

Biological locomotion systems are extremely diverse and are represented by many levels of organization, ranging from the mechanisms of movement of flagella in unicellular organisms to complex forms of locomotion such as flight [1, 2]. In this regard, mechanisms of biolocomotion are of significant applied interest, serving as a source for bioinspired and biomimetic approaches, e.g., in the fields of robotics and development of micro-electro-mechanical systems [3–5].

Actively moving animals use internal or external skeletons to maintain the shape of the body and limbs. The latter, as a rule, are composite and consist of several segments interacting through the joints. Thus, the joints are a key element in active locomotion, providing mechanical support and mobility to the limb. The limb joint in the simplest case consists of two contact surfaces moving relatively to each other by sliding or rolling. This interaction between the contacting surfaces is the subject of study in biotribology, where proper friction control plays a decisive role in the energetically effective motion and prevention of wear and fatigue.

The most common friction control strategy is lubrication, which is rather diverse in biological systems [6]. Lubrication-based friction control is the most extensively and thoroughly investigated for the vertebrate articular joints [7–10]. Having internal exoskeleton, the joints of vertebrates are encapsulated into isolated chamber filled out with synovial fluid and the friction minimization is based on the boundary lubrication that works synergistically with other mechanisms, such as pressurization-driven elastohydrodynamic lubrication [11]. This approach is highly effective, allowing friction coefficient to be reduced to extremely low values, reaching 0.02 for a stifle-joint in horses [12] and even an order of magnitude lower, from 0.005 to 0.023 for human joints [13, 14].

Arthropods, an enormously large group of animals, in contrast to vertebrates possess an external exoskeleton. Integument of joints comprises of fibrous-composite material called cuticle and, due to the fact that joints of arthropods are open to the environment and are not enchambered [15], the friction minimization for them is a challenge. Fluid-based lubrication, as in vertebrates, would not be effective in this case, due to the constant lubricant evaporation and to the high energy required for its producing. To cope with friction

✉ Konstantin Nadein
k.nadein@gmail.com

Alexander E. Filippov
filippov_ae@yahoo.com

Stanislav N. Gorb
sgorb@zoologie.uni-kiel.de

Alexander Kovalev
akovalev@zoologie.uni-kiel.de

[1] Department of the Functional Morphology and Biomechanics, University of Kiel, Am Botanischen Garten 1-9, 24118 Kiel, Germany

in leg joints, some arthropods developed a unique approach based on the solid or viscous-solid lubricants [16, 17].

As it is exemplified by the femoro-tibial joint in the darkling beetle *Zophobas morio* (Fig. 1a), the lubricant is represented by numerous particles in the form of short cylinders about 1 µm in diameter, unevenly covering the contact surfaces and emerging from the pore openings in the cuticle [16]. The lubricant material is protein-based and its tribological properties have been experimentally examined and reduced sliding friction to the value of 0.13 in the tribosystem 'glass/lubricant/glass' has been demonstrated [16].

Based on the scanning electron microscopy analysis, a speculative model of the lubrication has been proposed [16]. Two possible mechanisms, which may be responsible for the friction reduction with solid lubricant, have been proposed. (1) Cylindrical fragments of lubricant may experience rolling at the lower loads, when the gap between contacting surfaces is not smaller than 1 µm (a diameter of a lubricant fragment). (2) At the higher loads and when the gap between contacting surfaces is smaller than diameter of the lubricant fragments, the latter start experiencing plastic deformations and spreading over the surface preventing direct physical contact between joint surfaces. Thus, the minimization of a friction occurs both due to rolling (the friction in this regime is lower than sliding friction) and due to the creation of a layer separating the contact surfaces.

Direct experimental verification of this hypothesis in vivo seems to be rather difficult task, due to the very small size of the joints and even smaller lubricant particles themselves. At the same time, it seems possible to perform numerical simulation of the lubricant behavior and in this way to study its properties in contact. In particular, the rolling friction of cylindrical fragments may be modeled, which is presented in this paper.

2 Materials and Methods

2.1 Study Objects

Specimens of adult beetles of *Zophobas morio* (Coleoptera: Tenebrionidae) were taken from the colony keeping in the insectarium at the laboratory of Functional Morphology and Biomechanics at the Kiel University, Germany.

2.2 Scanning Electron Microscopy (SEM)

The observations were made at 3 kV using a Hitachi S4800 scanning electron microscope (Hitachi High-Technologies Corp., Japan). Legs from a freshly CO_2-anesthetized individual were cut off and dissected by razor blade in two halves in sagittal plane through a femoro-tibial joint, then dried out at the room temperature, glued to SEM stubs and subsequently coated with 10 nm gold–palladium layer using a Leica EM SCD500 sputter coater (Leica Microsystems GmbH, Wetzlar, Germany).

2.3 Micro-Computed X-ray Tomography (Micro-CT)

The scanning of the dry fore legs was carried out by a Sky-Scan 1172 (Bruker Corp., Billerica, USA) at 40 kV and 250 µA, with the camera pixel size of 8.8 µm and the image pixel size of 2.0 µm. 1573 projections were recorded over the 180° rotation. For 3D reconstruction, the graphic segmentation

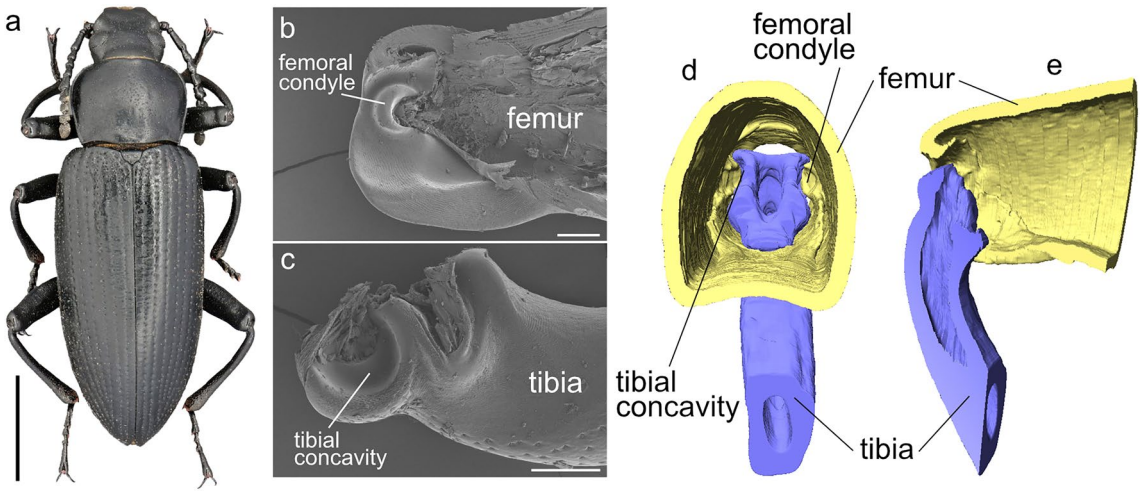

Fig. 1 The object of research, darkling beetle *Zophobas morio* and its femoro-tibial joint. **a** general appearance of *Zophobas morio*; **b** femoral counterpart, sagittal section, SEM micrograph; **c** tibial counterpart, lateral view, SEM micrograph; **d** femoro-tibial joint, view through femur, micro-CT volume reconstruction; **e** the same, sagittal section, micro-CT volume reconstruction. Scale bar: **a** 0.5 cm; **b**, **c** 200 µm (Color figure online)

tool software Amira® 6.2 (FEI Company, Visage Imaging, Germany) was used.

2.4 Numerical Simulation

Numerical simulations were performed in MatLab (MathWorks).

3 Results and Discussion

3.1 Structure of the Femoro-Tibial Joint of the Darkling Beetle *Zophobas morio*

The structure of the femoro-tibial joint has been previously described in details [16, 17]. Briefly the joint can be described as follows. Two counterparts are represented by the femur and tibia, respectively (Fig. 1b, c). The femoral counterpart bears two symmetrically placed condyles of semicircular shape, while the tibial counterpart possesses two invaginations called here tibial concavities. Correspondingly, the tibial concavities serve as sockets for the femoral condyles (Fig. 1d, e) and both counterparts are connected by tendons. The joint is uniaxial allowing rotation in only one plane defined by the surfaces of the femoral condyle and tibial concavities.

3.2 Lubricant

Lubricant material (Fig. 2) is represented by cylindrical fragments of various length (from about 1 µm to dozens of micrometers) resembling toothpaste. The diameter of the fragment is about 1 µm corresponding to that of the pores (Fig. 2a). The latter cover nearly the entire cuticle surface of the joint cavity and are counted to hundreds of individual pores. Lubricant fragments are often represented by comparatively short fragments of about 2–5 µm length (Fig. 2b–d) that can be arranged in regular groups forming a monolayer (Fig. 2b, c) or sometimes less arranged groups forming somewhat thicker layers (Fig. 2d). Such groups may cover large contacting surface area (Fig. 2e). Lubricants on the contacting surfaces (such as smooth surface of the femoral condyle and tibial concavity) are often represented by deformed flattened fragments spread over the surface (Fig. 2f).

3.3 Numerical Model of Lubricant in Femoro-Tibial Joint of *Zophobas morio*

Here we introduce a numerical simulation model, which geometry is based on our SEM observations. Generally speaking, behavior of the solid lubricant between contact surfaces can be simulated by the so-called "movable automata" confined between two moving rigid surfaces in 3D space. Main features of the system, which have to be

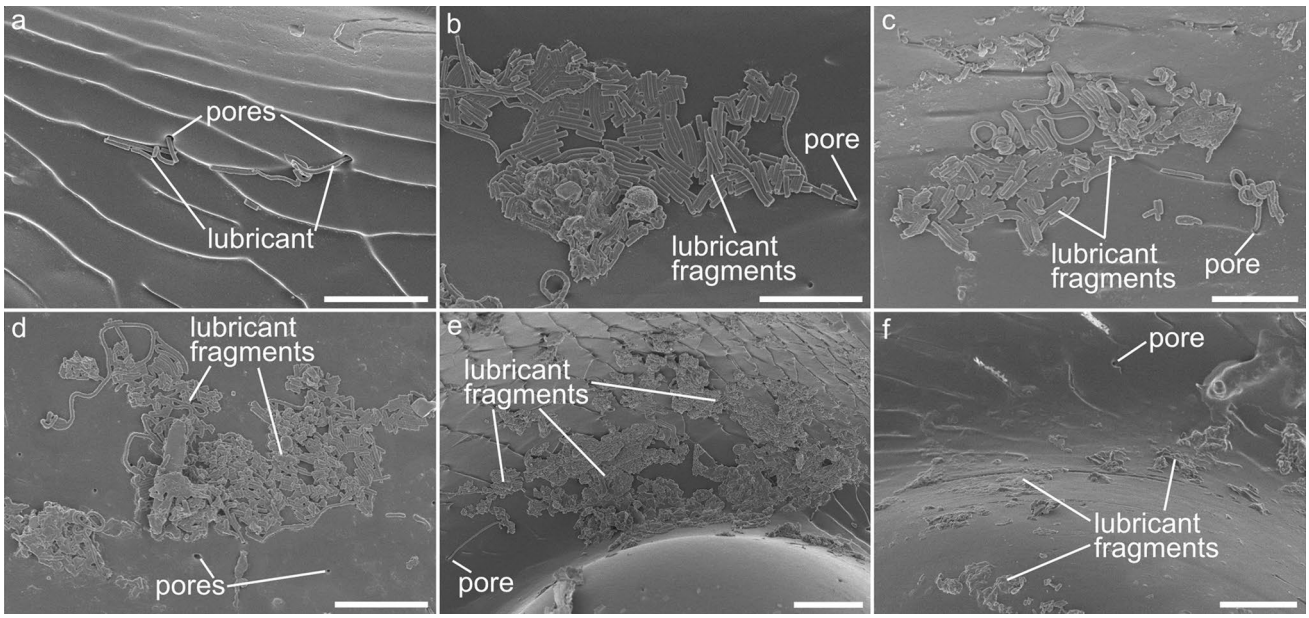

Fig. 2 Lubricant in the femoro-tibial joint of *Zophobas morio*, SEM micrographs. **a** lubricant coming out from pore openings; **b**, **c**, **d** assemblages of lubricant fragments over the contacting surfaces on the femoral counterpart; **e** large lubricant assemblages of various thickness covering contacting surfaces; **f** femoral condyle covered with lubricant fragments at various stages of deformation from weakly deformed to spread over the surface as a thin layer. Scale bars: **a**, **b**, **c** 10 µm; **d**, **f** 15 µm; **e** 20 µm

reproduced in the model frames, should include an external (e.g., gravitation) force acting on one of the surfaces (called "upper" below; the "lower" surface remains static) and shear force caused by motion of this ("upper") surface. Certainly, such a combination represents a standard tribological situation, which should be adapted to this specific biological case.

In particular, the system under consideration differs from many other ones by the time-dependent amount of the lubricant, which is gradually added into the space between the surfaces through the pores and redistributed in the gap between the surfaces in the course of some transient process, while a balance between the external pressure and bearing force, caused by the lubricant particles, will be reached. The lubricant particles combine the ability of irreversible plastic deformation and transverse stiffness which allows them to support upper surface against external pressure.

Such kind of particles was recently simulated in [18, 19]. The model used there describes a system of N particles represented by the vector radius $\mathbf{r}_i$, the momentum $\mathbf{p}_i$, and the interaction potential $U(|\mathbf{r}_i - \mathbf{r}_j|)$ corresponding to the following Hamiltonian:

$$H(\mathbf{r}_i, \mathbf{p}_i) = \sum_{i=1}^{N} \mathbf{p}_i^2/2m_i + \sum_{i,j=1}^{N} U(|\mathbf{r}_i - \mathbf{r}_j|)/2 \tag{1}$$

Technically it is convenient to represent the interaction potential by a pair of the Gauss potentials:

$$U(|\mathbf{r}_i - \mathbf{r}_j|) = C_{ij} \exp\{-[(\mathbf{r}_i - \mathbf{r}_j)/c_{ij}]^2\} - D_{ij} \exp\{-[(\mathbf{r}_i - \mathbf{r}_j)/d_{ij}]^2\} \tag{2}$$

where C_{ij} and D_{ij} define the magnitude, while c_{ij} and d_{ij} the radii of attraction and repulsion, respectively. The minimization condition corresponding to an equilibrium reads as follows:

$$C_{ij} >> D_{ij}, \quad c_{ij} < d_{ij} \tag{3}$$

The lubricant particles are confined between two planes: $z = 0$ (lower plane) and $z = L_z$(upper plane) with reflecting boundary conditions: $U_{up} = C \exp[(z - L_z)/c]$ and $U_{down} = C \exp[-z/c]$. The stronger the inequalities $C >> C_{ij}$ and $c << c_{ij}$, the more rigid and sharp are the "joint surfaces" in relation to other forces and lengths relevant to the system. Since the parameters C_{ij},D_{ij}, c_{ij}, and d_{ij} form arrays covering all possible combinations, it can be said without loss of generality that the Hamiltonian given by Eq. (1) describes systems with any number of components.

The equations of motion have the following form:

$$m_i \partial \mathbf{v}_i/\partial t = -\partial H(\mathbf{x}_i, \mathbf{p}_i)/\partial \mathbf{p}_i = \mathbf{f}_i \tag{4}$$

where $\boldsymbol{v}_i$ is the velocity of the i-th particle. All the uncontrollable influences, which normally exist in any biological system, should be incorporated according to fluctuation–dissipation theorem. It supposes an effective temperature T_{eff} which includes both real thermal bath and other stochastic random influences. It has to be included through random δ-correlated Langevin forces [20]. having the following correlators:

$$\left\langle \xi(t, x_i, y_i)\xi(t', x_j, y_j) \right\rangle = D\delta(t - t')\delta_{ij} \text{ and } \left\langle \xi(t, x_i, y_1) \right\rangle = 0 \tag{5}$$

where $D = 2\gamma k_B Tm/dt$, k_B is the Boltzmann constant, γ is a dissipation constant, and dt is the discrete time step.

Interacting lubricant particles exchange momentum mutually and with both upper (up) and lower surfaces. Hence, a dissipation channel acting to equilibrate the relative velocities of particles, that happen to be within the distance c_v close to the equilibrium, needs to be introduced. This was done by including an additive force

$$\mathbf{f}_i^v \sim \sum_{j=1}^{N} (\mathbf{v}_i - \mathbf{v}_j) \exp\left[-\left[(\mathbf{r}_i - \mathbf{r}_j)/c_v\right]^2\right]$$

$$\begin{aligned} f_i^v = &\sum_{j=1}^{N} (\mathbf{v}_i - \mathbf{v}_j) \exp\left[-\left[(\mathbf{r}_i - \mathbf{r}_j)/c_v\right]^2\right] \\ &+ (\mathbf{v}_i - \mathbf{v}_{up}) \exp\left[-\left[(\mathbf{z}_i - \mathbf{z}_{up})/c_v\right]^2\right] + \mathbf{v}_i \exp\left[-(\mathbf{z}_i/c_v)^2\right] \end{aligned} \tag{6}$$

on the i-th particle, with yet another dissipation constant η. As a result, the equations of motion assume the following form:

$$m_i \frac{\partial \mathbf{v}_i}{\partial t} = f_i^{\mathbf{r}} - \eta f_i^{\mathbf{v}} - \gamma \mathbf{v}_i + \xi(t, \mathbf{r}_i) \tag{7}$$

They were integrated using velocity Verlet's method, which conserves the energy of the system at each time step, provided no energy is supplied externally through the mechanical work or temperature variation.

In numerical experiments, particles are randomly produced inside a "cylindrical pore" of a radius $R >> c_{ij}$ at some rate. It is supposed that this cylindrical pore is oriented in z- direction (vertically). The lubricant particles being produced inside the cylindrical pore and extruded from it by a pressure, caused by the repulsion from particles produced later, went into the space between upper and lower planes. Here lubricant particles move confined between two horizontal planes separated by equilibrium width. This equilibrium width is determined by a balance of the external pressure (caused by a weight of an animal and other forces appearing due to the animal's motion). It is impossible experimentally determine the correct balance. Therefore, the typical scenario of the simulation was organized as follows.

1. At the beginning, the distance between planes was chosen sufficiently large to not hinder an initial lubricant generation;
2. When generation starts, an external pressure is applied to the upper plane along z-direction.
3. With a relatively short delay, we switch to the horizontal shear motion of the upper plane along y- direction;
4. Normally, the shear stress caused by this horizontal motion bends a column of the lubricant extruded to this moment and presses it down to the substrate, where the pore is situated. This process strongly reminds experimentally observed bended lubricant strands (see for example photo in Fig. 2a, c);
5. Due to limited transversal and longitudinal rigidities of the viscous lubricant material, the strand splits into shorter fragments. Being split, the lubricant pieces move separately. They bend, interact one with another, and reorder. At some conditions, they even collide and build larger pieces of quite general form and split into pieces again. The form, size and other properties of these clots are determined by a balance between all the forces in the system under consideration.

Such possibility is naturally incorporated into the model using 'movable automata' Eqs. 1–3 (see also the paper [21] and book [22]). This approach has been applied here to the system under consideration. We have simulated rather realistic configurations of the present system, which incorporates (1) the continuous lubricant production, (2) vertical and tangential motions of all the system components, (3) as well as dynamically established and permanently maintained further self-consistent dynamic balance for all the forces of the system under consideration. The results of the preliminary simulations are briefly summarized in the Supplementary Movie 1. It reproduces well the majority of the system properties of the real observed biological joints presented in the Introduction.

In particular, a flux of the lubricant substance, which is continuously generated from the pore, is well seen in the movie. The lubricant substance spontaneously forms "cylinders" and "knots," which slide, rotate and either collide and build larger ones or become smeared into wider patches under external pressure acting on the upper surface. Besides, one can notice in the movie some "channels" on the surface, which affect all the mentioned processes and may favor optimal regulation of the friction in the system. Despite of the rather realistic behavior achieved using 'movable automata' approach mentioned above, it is sufficiently time-consuming and needs a long-time runs to perform all necessary studies at different regimes and parameter combinations.

One has to note also that in general case the contact surfaces are not ideally planar. However, as it was experimentally shown, they are structured and this structuring might have a biological importance. Numerical experiments demonstrate that, if the surfaces are not structured, at periodic oscillations of the upper surface, the lubricant produced from a local pore moves along the same trajectories and accumulates into large snowballs (sometimes spherical, sometimes cylindrical, or even formless). Surface channels, which do not cross the holes directly, are not parallel to the motion direction of the upper surface and due to the properly adjusted depth, help for better separation of the lubricant material into relatively short and more or less cylindrical regularly rotating fragments.

In other words, the rotation of quasi-cylindrical pieces of the lubricant is important component of their motion. This observation let us simplify the model and significantly reduce the time necessary for simulations. Further, we describe how the simplified version of the model was constructed and utilized in the present study.

First, the cylindrical particle agglomerates were modeled as tubes. In the simplified version of the model the initial distribution of the tubes was simulated by the lubricant secretion process as follows: at the beginning, one elastic tube is produced from a pore in the lower surface. After the extruded tube reaches a specified length, it splits into a number of the separate tubes, when vertical pressure and shear force caused by horizontally pulled upper surface exceed some critical threshold. Later on, the individual tubes cannot be split in the framework of the simplified model. They move quasi-independently, but interact and collide one with another as well as with both surfaces. Due to all of these interactions, the tubes order themselves with their main axes perpendicular to the motion direction of the upper plane and their own motion, and (more or less efficiently) rotate around their main axes. As a result, the whole system acts as a kind of "friction bearing." Moreover, the case presented in the simplified model could be also observed in the real beetle leg joint at the high stress and small gap between upper and lower surfaces (as in Fig. 2b, c). One can expect that such an effect plays some role in a reduction of the friction in real insect joints.

Conceptual structure of the model is reproduced in Fig. 3. To simulate flexible lubricant particles, we constructed them as follows. Basically, we apply the same equations of motion, boundary and initial conditions as described above (see Eqs. 1–7). However, instead of modeling of the interacting lubricant particles, we modeled the motion of independent tubes from the very beginning. Each tube is generated by an elastic cylindrical surface formed in 3d space by folding of the planar rectangular grid (mesh) of the connected segments. Each node of the grid interacts with other ones by a nonlinear elastic force which tends to conserve initial distance between the nodes in originally constructed structure. It means that instead the simple combination of the attracting and repulsion

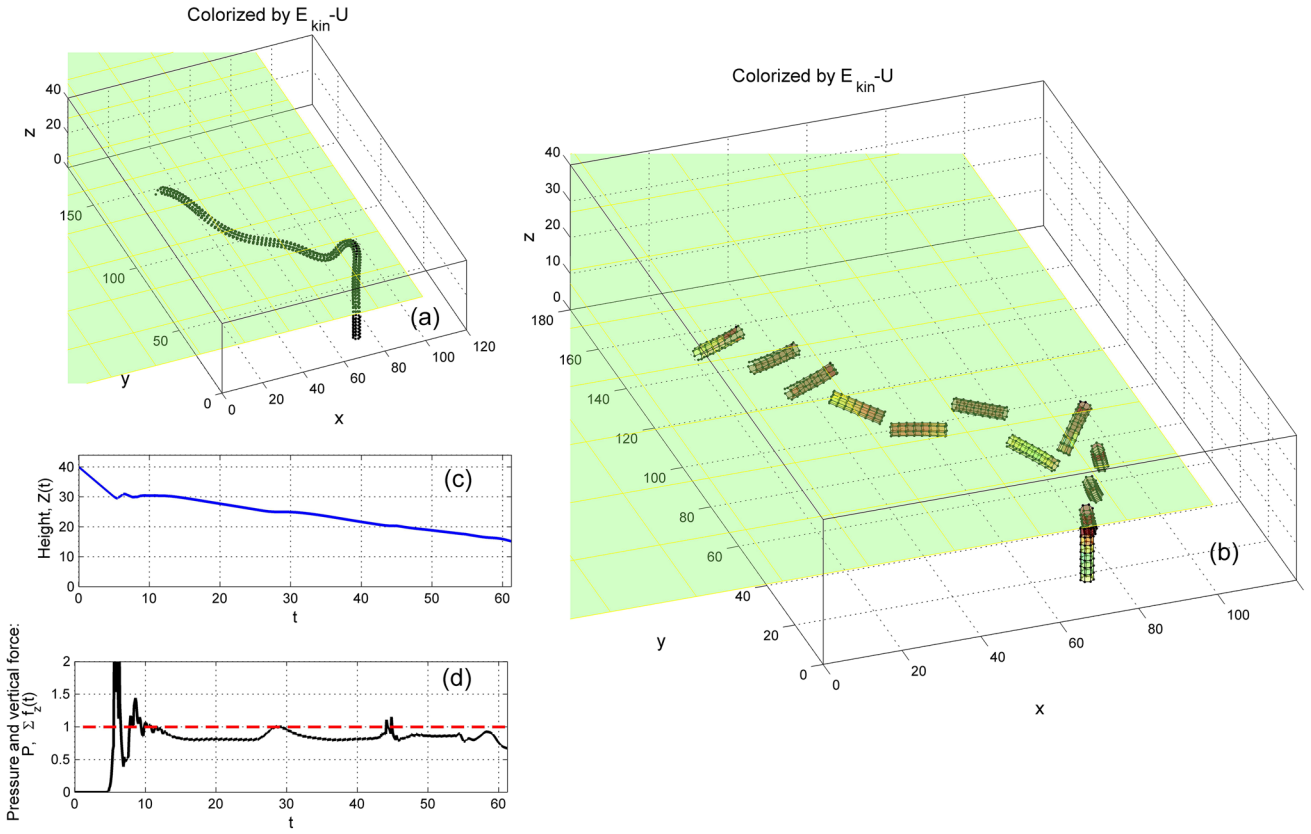

Fig. 3 Early stages of the numerical experiment. Subplot **a** reproduces solitary long tube, growing from a pore (is not shown in the picture) pressed and sheared by the motion of the upper surface (shown by a part of semi-transparent plane above the tube). **b** The same tube being split into a number of the moving short pieces. Here and below all the movable surfaces are colored in standard MatLab 'jet' colormap according to the difference between instant spatially distributed kinetic $E_{kin}(\vec{\mathbf{r}},t)$ and potential $U(\vec{\mathbf{r}},t)$ energies (which make visible position height z of each surface segment and its' deformation amplitude). Time depending vertical position of the upper surface $Z(t)$ as a balance between the vertical forces $P(t)$ and $\sum_{j=1}^{N} f_z^j(\vec{\mathbf{r}},t)$, corresponding to the depicted here initial stage of the process, are shown in the subplots (**c**) and (**d**), respectively (Color figure online)

components of the potential $U(|\mathbf{r}_i-\mathbf{r}_j|)=C_{ij}\exp\left\{-\left[(\mathbf{r}_i-\mathbf{r}_j)/c_{ij}\right]^2\right\}-D_{ij}\exp\left\{-\left[(\mathbf{r}_i-\mathbf{r}_j)/d_{ij}\right]^2\right\}$, which guarantees quasi equilibrium distance between randomly moving lubricant particles only in average, we maintain the distances between the particles in the originally prescribed tubes:

$$U_{\text{elastic}}(|\mathbf{r}_i-\mathbf{r}_j|)=K_{ij}\exp\left\{-\left[(\mathbf{r}_i-\mathbf{r}_j)/r_k\right]^2\right\}\left[1-\left[(\mathbf{r}_i-\mathbf{r}_j)/a\right]^2\right\} \tag{8}$$

This potential automatically keeps the nodes inside every tube always connected one with another with a characteristic constant close to an "equilibrium distance" a. Such interaction provides the stability for each separate tube, and imparts them effective longitudinal and lateral stiffness. As a result, the tubes can move stably, collide one with another, rotate as mesoscopic "bodies" having correct shape and stiffness, but cannot disappear or irreversibly deform.

This modification of the model strongly reduces computational time, because one should not calculate interactions of every particle inside a tube with all the other particles, but only with some limited number of them formally describing the surfaces via interacting nodes. In some sense, we deal here with interacting "empty tubes" having effective parameters which mimic properties of the real cylindrical particles' agglomerates. Effective stiffness of the tubes, automatically appearing in such a model plays very important role in separation of the upper and lower surfaces at an external pressure due to the tubes' stiffness.

All the features of the process found during typical simulation scenarios are summarized in the Supplementary Movies 2 and 3. In particular, Supplementary Movie 2 reproduces generation of a long flexible tube, which starts to grow vertically from a pore in the lower surface. To get correct (initially unknown) equilibrium position of the upper surface we start its motion rather far away from the lower one. The upper surface moves down, until it will be stopped by a resistance of the lubricant between the surfaces. In turn, the

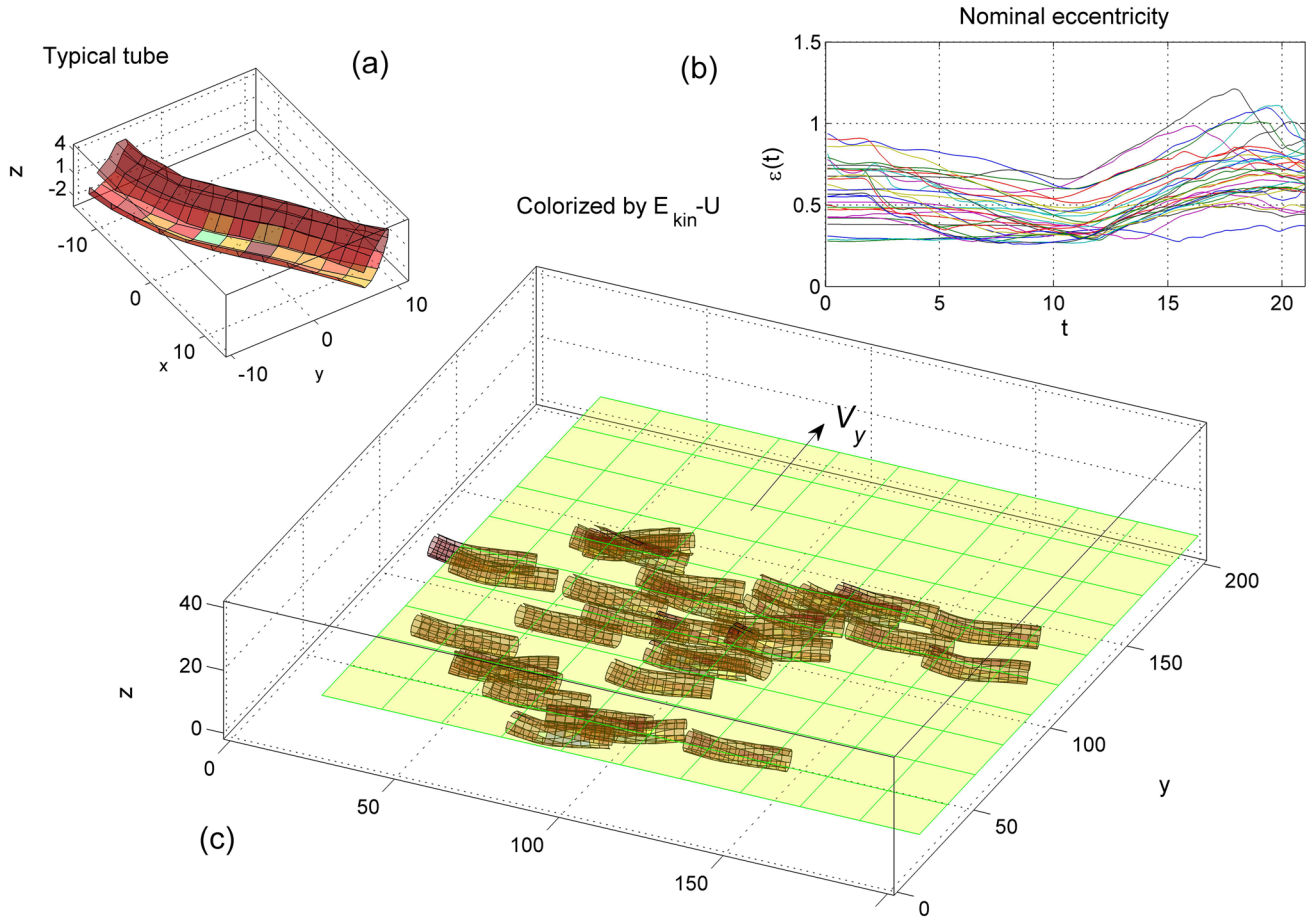

Fig. 4 Typical intermediate stage of the numerical experiment. Majority of the tubes are squeezed between the upper and lower surfaces and tend to become more or less parallel one to another being oriented along x- axis (perpendicular to the shear, which is for definiteness directed along y- axis with velocity V_y). Originally, all the tubes are supposed to be perfect cylinders, $\epsilon(t=0)=1$. Some of the tubes become deformed by mutual interactions and all of them are deformed by vertical pressure. Typical deformed tube is shown in the subplot (**a**). In general case, the vertical pressure causes a decrease of the eccentricity $\epsilon_{effective}(t)$ of the tube cross section. Due to random orientation, they typically have an elongated projection along y-axis. Thus, formally calculated $\epsilon_{effective}(t)$ varies with the time. The family of such time dependencies is plotted in the subplot (**b**). Instant configuration of the tube ensemble is reproduced in the subplot (**c**) (Color figure online)

surfaces interact with the lubricant tubes and influence their positions. Balance of the interactions stops vertical motion of the upper surface and holds it in instant equilibrium. At the same time, interaction with both surfaces force the tube splitting into a number of short fragments. The patterns observed during the splitting process correspond qualitatively well to the images observed experimentally Figs. 3, 4, and 5.

In the static form, different stages of the simulated process are reproduced in Figs. 3, 4, 5, 6, 7, and 8. Initial formation of the lubricant tube, extruded from a pore in the lower surface, is reproduced in the subplot (a) of Fig. 3. In this subplot, one can see a solitary long tube extruded almost vertically. Here and below, we associate this direction with z-axis. The pore producing the lubricant is not shown in the picture and it is not incorporated directly to the model. Technically, the generation of lubricant is simulated by adding of new segments of the tube with the time t. For a simplicity, the generation in the framework of the model continues up to some moment $t_0 > 0$. Then, the generation is formally stopped and only horizontal motion of the upper surface serves as a source of the energy for the mobility of the system elements. Additionally, for a definiteness and simplicity, a constant vertical force (external pressure $P = -F_{ext}$) acts during the whole process. It also causes generation of a kinetic energy in the system, which is basically produced up to some moment, when a balance between the vertical forces is established.

The creation of new segments of the lubricant tube (and consequently increasing number of separate lubricant tubes later on after fragmentation of the original one) leads to a

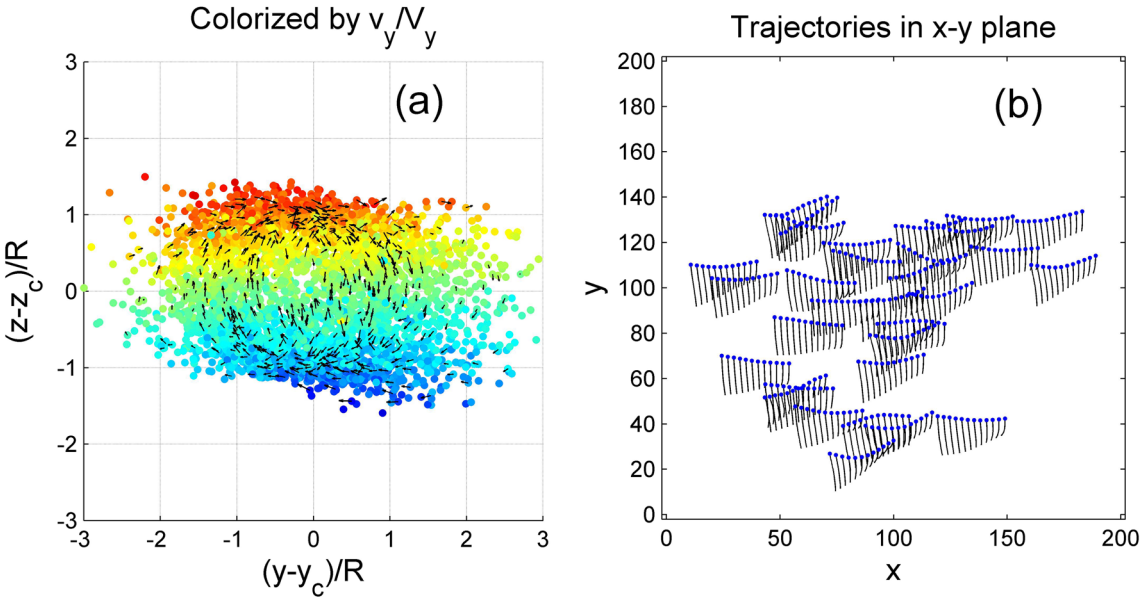

Fig. 5 The phase portrait for all the nodes in the system, projected to the plane $\{z - z_c, y - y_c\}$, is shown in the subplot (**a**). Arrays $\{z_c, y_c\}$ are defined here by the centers of mass for each tube. The vector field of the node velocities is accompanied by the scatter plot of the node positions colored by the value of an individual velocity. Blue color corresponds to the almost zero velocities of the nodes close to the motionless lower surface. Red one corresponds to the nodes, which are close to the upper surface and move with the shear velocity V_y. Due to the interactions one with another and with the surfaces, the tubes gradually line up along the direction x. This process is illustrated in the subplot (**b**) by the families of the comet-tails showing short parts of the segment trajectories (Color figure online)

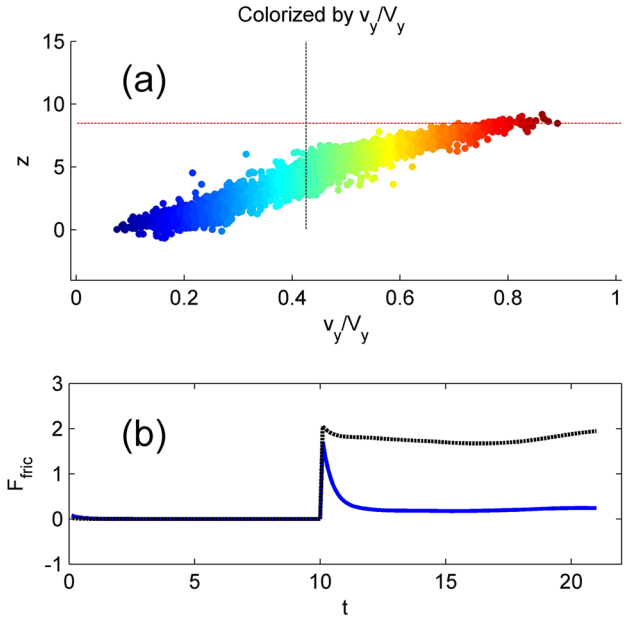

Fig. 6 Friction reduction due to the rotation of tubes. All the tube nodes (for many tubes) are shown by their projection into the plane $\{z, v_y/V_y\}$ in the subplot (a). They are colored in the same manner as in the Fig. 5. Time dependence of the total friction, which is calculated by accumulation of the total losses in the system (see main text), is plotted as blue solid line in the subplot (b). Formally calculated friction of the system, which slides without rotation with the velocity of the center of mass marked by vertical line in the subplot (a) is presented in the subplot (b) by the dotted black line for a comparison (Color figure online)

grow of the collective force $F^z = \sum_{k=1}^{N} f_k^z$, which approximately balances the external pressure $F_{ext} \approx \sum_{k=1}^{N} f_k^z$ at later stationary stage of the process $t >> t_0$. However, strictly speaking this balance never reaches the equilibrium $F_{ext} = \sum_{k=1}^{N} f_k^z$. It is always maintained only approximately by the creation of new segments, collisions between existing tubes, and by their deformations. Certainly, the perturbations are stronger pronounced at early stages. General tendency leads to a minimization of these fluctuations accompanied by ordering of the interacting tubes into more or less parallel set, which stationary rotates. In this limit, the tubes are mainly ordering perpendicularly to the shear direction, and distributing in one thin layer (without large deformations and multilayer packaging).

Such a behavior perfectly matches to that seen in microscopic observations of beetle joints. Below we show that analogous behavior is rather naturally reproduced by the model. In turn, such agreement between the model and observations allows applying our model to study other features of the real system, which either cannot be directly measured or even observed at the current state of experimental technology.

In Fig. 3a, the movable upper surface is shown by a part of semi-transparent plane above the growing tube. When a

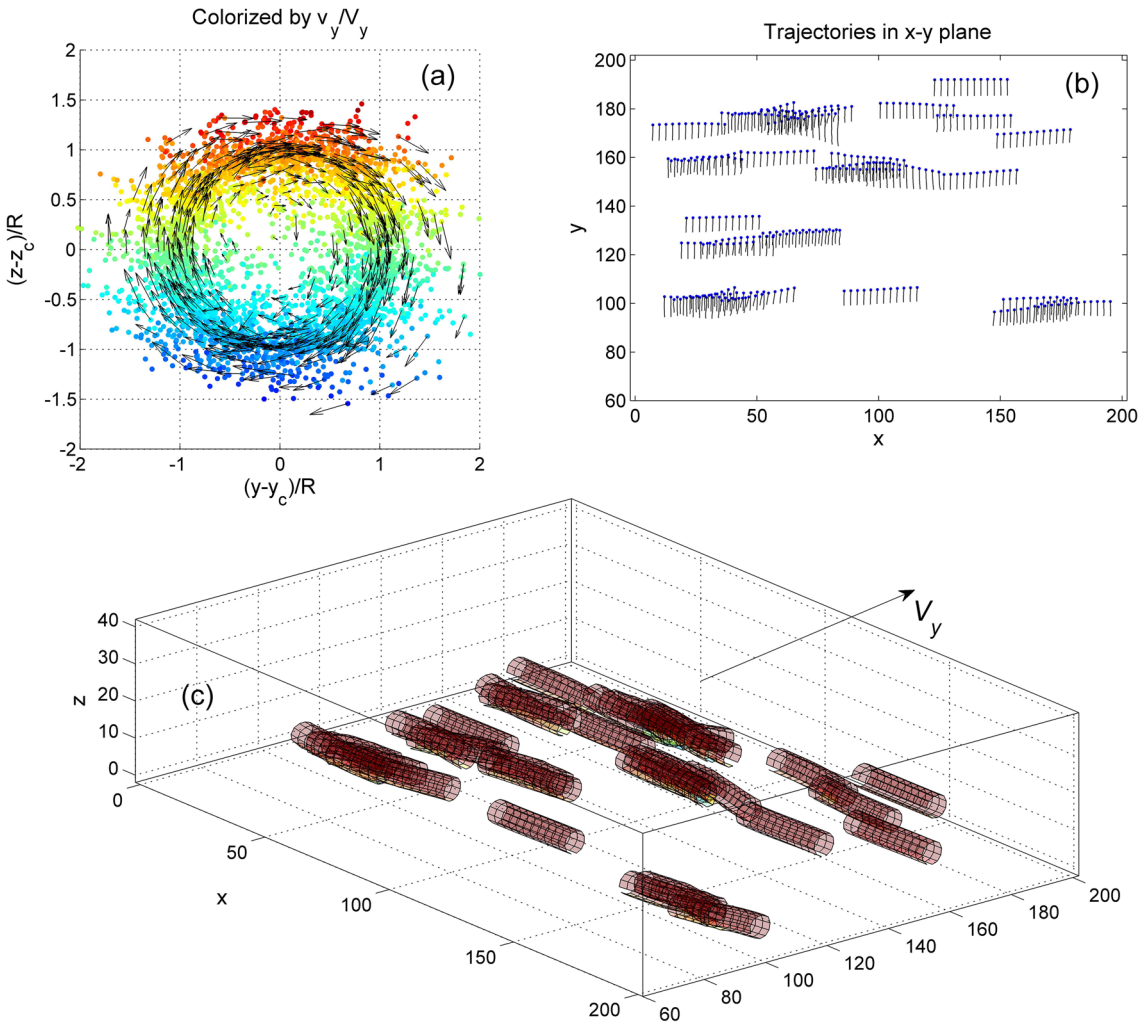

Fig. 7 The phase portrait for all the nodes in the system, projected to the plane $\{z - z_c, y - y_c\}$, is shown in the subplot (**a**). This plot is the same as in Fig. 5, but obtained at late, almost stationary stage of the process, when all tubes are aligned along x-axis. The phase portrait of all the tubes together, shown in the subplot (**a**), has well defined hole in the projection to the plane $\{z - z_c, y - y_c\}$. The vector field of the velocities is almost perfectly circular. Comet tails in the subplot (**b**) are practically parallel one to another. It means that the majority of the tubes spin in parallel in the direction of the external velocity V_y. Instant picture of such almost ideal motion in 3D space is reproduced in the subplot (**c**) (Color figure online)

stress, caused by combined forces of vertical pressure and horizontal motion of the surface, exceeds some threshold, originally solitary tube splits into a number of the (quasi-) independently moving relatively short pieces. Here and below all the movable surfaces are colorized in standard MatLab 'jet' colormap according to the difference between instant local kinetic $E_{kin}(\vec{\mathbf{r}}, t)$ and potential $U(\vec{\mathbf{r}}, t)$ energies. Besides, all such particle surfaces are semi-transparent. It allows us making visible different features of this (combinatorially) complex system simultaneously. In particular, the difference between kinetic and potential energies allows visualizing both: the height (z) of every surface segment, its velocity and amplitude of the local deformation. To illustrate this, we spatially magnify one of the arbitrary chosen separate tubes in the subplot (a) of Fig. 4. One can follow the deformations of the tube and corresponding variations of the colors in the Supplementary Movie 2.

Time depending vertical position of the upper surface $Z(t)$ as a balance between the vertical forces $P(t)$ and $\sum_{j=1}^{N} f_z^j(\vec{\mathbf{r}}, t)$, corresponding to the depicted here initial stage of the process, are shown in the subplots (c) and (d) of Fig. 3, respectively. As intuitively expected, the vertical pressure leads to a gradual lowering of the upper surface. In average, it is monotonous up to the establishing of the approximate equilibrium. However, due to the random impacts from plenty of the interacting subsystems, seen in the subplot (d) rather

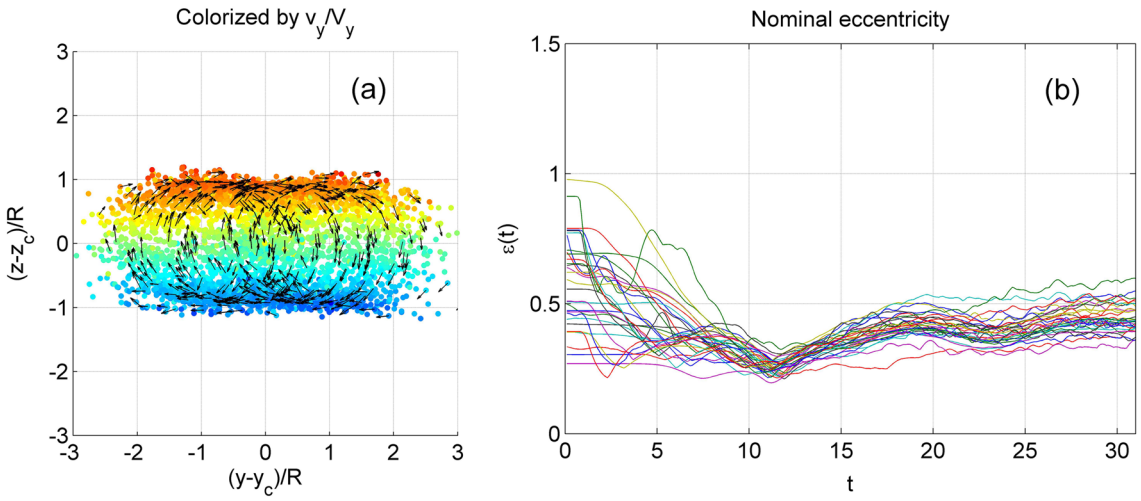

Fig. 8 The deformed phase portrait (**a**) and curves family of time-dependent eccentricity (**b**) found in the case of a strong vertical pressure. The difference with almost ideal circular rotation at small pressure, reproduced in the previous Fig. 7 is seen directly (Color figure online)

pronounced fluctuations of the height with time are seen as well.

At the first glance, these fluctuations of the clearance between the surfaces have only academic meaning. One can expect that if the lubricant volume (number of the tubes) is large enough, the fluctuations should become negligibly small. However, it seems that in reality the amount of lubricant (density of local spots of it) is not so high. In some places, or at some time intervals, this amount can be extremely small and intermediate supporting layer between rough hard surfaces can practically disappear. This effect can play a very important role in such cases. Thus, it is important to take into account the mentioned fluctuations of an unevenly distributed substance in the model consideration.

Independent problem of the static visualization of expected and practically useful results of numerical experiments is caused by a combination of uneven tube distribution and interaction between tubes. Direct observation of the rotation and ordering of the tubes can be statically analyzed by projecting of all their nodes into projection on some hyperplanes (phase portraits). For example, one can accumulate the nodes coordinates relative to the center of mass for each tube in one phase portrait. Such phase portrait for all the nodes of the system, in the projection to the plane $\{z - z_c, y - y_c\}$ is presented in Fig. 5a. Here, array $\{z_c, y_c\}$ represents the coordinates of the centers of mass of each tube. One can project also all the velocities into the same plane. It gives a vector field of the velocities of the nodes. Besides, the information about the value of node velocities can be integrated in the same plot by color. In the subplot (a), blue color of the nodes corresponds to minimal (almost zero) velocities, which are normally situated close to the motionless lower surface. Red color corresponds to the quickly moving nodes which, as a rule, are closer to the uppers surface. They move at almost shear velocity V_y.

Interactions between the tubes and between the tubes and the surfaces lead to the tube reorientation. The tubes gradually line up along direction x perpendicular to V_y. This biologically important effect is illustrated in Fig. 5b by the families of the comet-tails showing short parts of the segment trajectories. Such parallel reorientation is observed in SEM images of the lubricant (Fig. 2). Such reorientation might favor to the work of the joint system with lubricant as an effective "friction bearing."

The friction reduction due to the rotation of the lubrication tubes is illustrated in Fig. 6. As above, all the tube nodes (for many tubes) are situated in one hyperplane of the system. For demonstration of the friction reduction, it is reasonable to represent the nodes in the phase space $\{z, v_y/V_y\}$ (Fig, 6a). The node projections are colored in the same manner as in Fig. 5. The friction in the system can be calculated by accumulation of the total energy loss. To do this, we calculate the work produced by the forces acting on each particle of the system or the corresponding power $p_i = \mathbf{f}_i \mathbf{v}_i$. Summation over all nodes yields the total power:

$$VF_{friction}(t) = P(t) = \sum_{i=1}^{N} \mathbf{f}_i \mathbf{v}_i \tag{9}$$

extended by an external friction force to maintain the motion of the boundary surfaces with a constant velocity, $V = const$. This yields the total force, $F_{friction}(t)$.

Total friction force shown as blue solid line in Fig. 6b demonstrates a sharp maximum, which corresponds to the "static friction" observed at the beginning of the shear motion of the upper surface. It gradually reduces, when

the majority of tubes aligns perpendicularly to the shear direction and starts to rotate. In stationary process, the segments of the tubes, situated close to both surfaces, mainly move with the velocity close to the particular surface and the losses are minimal. For a comparison, the friction is formally calculated for the frictional system, which slides without rotation with the velocity of the center of mass (marked by vertical line in Fig. 6a). The result of this calculation is presented in the subplot (b) by the dotted black line. Frictional force in this case (dotted black curve) is obviously higher than in the case of the rotating tubes (solid blue curve) (Fig. 6b).

Basically, the difference between the forces for scenarios with and without rotation originates from the spatial distribution of the velocity in the presence of rotation. In both cases, the tube moves with an average velocity of all its nods close to a half of the velocity of the upper surface. However, energy loses due to the friction appear from the difference between the velocity of the surface and the local velocity of the tube nodes near to the contact of the tube with the surface. When the rotation is undisturbed, this local velocity almost coincides with the surface velocity and the friction formally tends to zero. In opposite limit, when the tube slides, this difference is maximal. In all realistic intermediate cases, the friction is different, but in any case, it is generally lower than at pure sliding.

Small separate tubes continue their motion under horizontal shear force caused by the motion of the upper surface relatively to the lower one. Physically, this force results from the local friction between every node of the tubes situated close to the surface and the surface itself. Phenomenologically, that is why the friction velocity of the lubricant particles near the surface tends to be equal to the surface velocity. The interaction between every node of the tube and closest point of the surface exponentially decreases with the distance.

The most remarkable and biologically important side of this phenomenon is that the friction force turns the tubes into rotational motion and alignment. In general case, especially at an intermediate stage of the process, the tubes do not lie in the plane parallel to the surfaces. In principle, they can rotate around any arbitrary chosen axis in 3D space. Instantly, some of the tubes even tumble around their short axis. However, the tumbling is typically just decent and slow reorientation of the longest axis of all tubes perpendicular to the direction of the upper surface sliding takes place. To visualize this reorientation in the static pictures, we have plotted short parts (so-called comet tails) of the trajectories of the seams coming along each tube. Such comet tails, and the reorientation of the tube seams perpendicular to the shear direction are seen in Fig. 7.

Despite of the correct direction of the lubricant tubes in stationary configuration, their rotation and corresponding minimization of the friction still has to be proven in numerical experiments. As mentioned above, the equilibrium position of the upper surface is determined by a balance between external forces and lubricant stiffness. The tubes are deformed under the pressure and in general case change their form. Eccentricity of their cross-section under pressure may serve as a measure for such deformation. The further the cross section deviates from the ideal circle, the more energy is required for the tube spin, the higher is the friction. Deformed phase portrait and curves family of the eccentricity time dependence shown in Fig. 8 (subplots (a) and (b), respectively) are observed in the case of strong vertical pressure. The difference with almost ideal circular rotation at small pressure is well reproduced above by the model.

4 Conclusion

The proposed model in a simplified form describes and simulates the state of the tribosystem of the leg joint, in which the contact surfaces are separated by lubricant fragments. It is shown that when surfaces move relative to each other, lubricant fragments can change their orientation to a more ordered one. In conditions where the distance between the contact surfaces is close to the size of the cylindrical lubricant fragments, the latter may experience rolling motion. Larger conglomerates of lubricant fragments can roll in a similar manner. In general, the presence of spacers (lubricant in the present case) between the contacting surfaces and their rolling allows the tribosystem to significantly reduce friction due to the predominance of rolling friction, as is the case in bearings. At the same time, the model demonstrates the possibility of other states of the tribosystem, in which fragments can experience plastic deformation and sliding friction becomes the predominant type of friction.

The presented model shows significant similarities between the results of numerical simulation and observational data obtained from studying a real leg joint, for example in the presence of an ordered orientation of individual lubricant fragments. The proposed model can claim to be a fruitful and promising approach to describe the tribosystem of a real leg joint in insects under conditions of dry friction and solid–solid contact. Also, the modeling results allow us to take an optimistic approach to assessing the previously proposed hypothesis about the mechanism for reducing friction in the joints of the legs due to the rolling of lubricant fragments as one of the cases occurring in this tribosystem [16]. Notably, the idea of using micro-fragments (essentially micro-bearings) to simulate rolling motion between contacting surfaces is being actively explored and showing promising results, such as in a study on micro-spheres as an additive to liquid lubricants [23]. Complemented by data from the study of biological tribosystems, as in the case of

the insect leg joint, such researches may stimulate further efforts in the fields of biomimetics and materials science, with particular benefit for the development of micro-electro-mechanical devices and micro-joints for robotics.

Supplementary Information The online version contains supplementary material available at https://doi.org/10.1007/s11249-023-01815-3.

Author Contributions All the co-authors initiated and designed the study. AF created the numerical model, which was validated by KN and AK. AF created part of illustrations. KN studied the model object, made observations, measurements, and part of illustrations. AF and KN wrote the manuscript. All the co-authors revised the manuscript.

Funding Open Access funding enabled and organized by Projekt DEAL. The work of KN is supported by the German Research Foundation (DFG project'Functional design of beetle leg joints: morphology, tribology, and cuticular microstructure', NA 126472-1 and DFG project 'Arthropod leg joints as biological devices: design, mechanical properties and anti-friction mechanisms', NA 1264/3-1). The work of AF is supported by the Humboldt Foundation. The work of SG is supported by the German Research Foundation (DFG Grant GO 995/38-1).

Data Availability The data that support the findings of this study are available from the corresponding author upon reasonable request.

Declarations

Conflict of interest The authors declare no conflict of interest.

References

1. Taylor, G.K., Thomas, A.L.R.: Evolutionary biomechanics: selection, phylogeny, and constraints. Oxford University Press, Oxford (2014)
2. Alexander, D.: Nature's machines: an introduction to organismal biomechanics. Elsevier Academic Press, London (2017)
3. Wilson, R.: Biomimetic robotics. Willford Press (2016)
4. Webb, B.: From insects to robots. Arthropod Struct. Dev., Special Issue **46**, 687–752 (2017)
5. Persiani, S.: Biomimetic of motion: nature-inspired parameters and schemes for kinetic design. Springer Cham (2018)
6. Greene, G.W., Lee, D.W., Das, S., Banquy, X., Israelachvili, J.N.: Lubrication and wear protection of natural (bio) systems. In: Zeng, H. (ed.) Polymer adhesion, friction, and lubrication, 1st edn., pp. 83–133. John Wiley & Sons Inc, Hoboken (2013)
7. McCutchen, C.W.: The frictional properties of animal joints. Wear **5**, 1–17 (1962)
8. Wright, V., Dowson, D.: Lubrication and cartilage. J. Anatomy **121**, 107–118 (1976)
9. Huber, M., Trattnig, S., Lintner, F.: Anatomy, biochemistry, and physiology of articular cartilage. Invest. Radiol. **35**, 573–580 (2000)
10. Klein, J.: Molecular mechanisms of synovial joint lubrication. Proc. Inst. Mech. Eng. Part J, J. Eng. Tribol. **220**, 691–710 (2006)
11. Ruggiero, A.: Milestones in natural lubrication of synovial joints. Front. Mech. Eng. **6**, 52 (2020)
12. Jones, E.S.: Joint lubrication. Lancet **223**, 1426–1427 (1934)
13. Chamley, J.: The lubrication of animal joints in relation to surgical reconstruction by arthroplasty. Ann. Rheumatic Dis. **19**, 10–19 (1960)
14. Fung, Y.C.: Biomechanics: mechanical properties of living tissues, 2nd edn. Springer, Berlin (1993)
15. Chapman, R.F.: The insects: structure and function, 5th edn. Cambridge University Press, New York (2013)
16. Nadein, K., Kovalev, A., Thøgersen, J., Weidner, T., Gorb, S.: Insects use lubricants to minimize friction and wear in leg joints. Proc. R. Soc. Biol. Sci. **288**, 20211065 (2021)
17. Nadein, K., Gorb, S.: Lubrication in the joints of insects (Arthropoda: Insecta). J. Zool. **316**, 24–39 (2022). https://doi.org/10.1111/jzo.12922
18. Beygelzimer, Y., Estrin, Y., Filippov, A., Mazilkin, A., Mail, M., Baretzky, B.: Simulation of layered structure instability under high-pressure torsion. Mater. Lett. **324**, 132689 (2022)
19. Beygelzimer, Y., Filippov, A., Estrin, Y.: Turbulent' shear flow of solids under high-pressure torsion. Phil. Mag. **103**, 1017–1028 (2023)
20. Langevin, P.: Sur la théorie du mouvement brownien [on the theory of brownian motion]. C. R. Acad. Sci. Paris. **146**, 530–533 (1908)
21. Dmitriev, A.I., Nikonov, A.Y., Filippov, A.E., Psakhie, S.G.: Molecular dynamics study of the evolution of rotational atomic displacements in a crystal subjected to shear deformation. Phys. Mesomech. **22**, 375–381 (2019)
22. Filippov, A.E., Gorb, S.: Combined discrete and continual approaches in biological modelling. Springer, Switzerland (2020)
23. Ma, X., Gan, C., Li, X., Li, Y., Feng, P., Fan, X., Ye, X., Zhu, M.: Tribological properties of SiO_2@Cu and SiO_2@MoS_2 core-shell microspheres as lubricant additives. Tribol. Lett. **69**, 108 (2021)